

Simulation of Turbulent Flow of a Rotating Cylinder Electrode and Evaluation of its Effect on the Surface of Steel API 5L X-56 during the Rate of Corrosion in Brine Added with Kerosene and H₂S.

P. Atempa-Rosiles¹, M. Díaz-Cruz^{1,}, A. Cervantes-Tobón¹, J. L. González-Velázquez¹, J. G. Godínez-Salcedo¹, Y. A. Rodríguez-Arias², R. Macías-Salinas³.*

¹ Instituto Politécnico Nacional, Departamento de Ingeniería Metalúrgica, Laboratorios Pesados de Metalurgia UPALM, Col. Zacatenco, Del. G. A. Madero, 07738, México, D.F.

² Instituto Politécnico Nacional, SEPI-ESIME, UPALM, Col. Zacatenco, Del. G. A. Madero, 07738, México, D.F.

³ Instituto Politécnico Nacional, Departamento de Ingeniería Química, UPALM, Col. Zacatenco, Del. G. A. Madero, 07738, México, D.F.

*E-mail: mdiazc@ipn.mx

Received: 22 April 2014 / Accepted: 30 May 2014 / Published: 16 June 2014

This work is based on the simulation, through ANSYS Fluent software, of turbulent flow induced by a rotating cylindrical electrode. It was carried out a 2-D Hydrodynamic simulation using the standard turbulence models k- ϵ and k- ω , the results on the velocity field clearly show the formation of turbulent Taylor vortex flow. The flow accelerated corrosion rate effect on the surface of the API 5L-X56 Steel was assessed using a brine of kerosene and H₂S. Corrosion products formed were characterized with Scanning Electron Microscopy (SEM), Electron Dispersive X-ray (EDX), X-ray Diffraction (XRD) and Linear polarization technique. XRD analysis showed that the corrosion products are mainly composed of a mixture of oxides and sulfides.

Keywords: Rotating cylinder electrode (RCE), API 5L-X56, Turbulent flow, ANSYS simulation.

1. INTRODUCTION

Accelerated corrosion flow dissolved the protective oxide film so fast how it forms or prevents its formation, causing corrosion of the unprotected surface. Therefore, the dissolution of the protective oxide film and an electrochemical attack occurs simultaneously and the continuous loss of material takes place. The Flow Assisted Corrosion (FAC) is produced from relatively low speeds, involving

laminar and turbulent flow. For pipes manufactured of carbon steel and low alloy steel, the results of flow assisted corrosion is the thinning of the internal walls of the pipe. Most of the current studies are based on the analysis of corrosion caused by CO₂ or H₂S under individual basis [1]. It is extremely important to carry out studies that consider analysis of the corrosion rate and the effect of the flow rate of fluid, since it has been reported to be some of the most significant parameters in the corrosion process. [2].

It has been developed a methodology for obtaining mathematical models that predict the corrosion rate for a particular system. This methodology involves some operating variables such as pH, temperature, pressure, aerated or deaerated media, with and without corrosion products. Analyzing the effects of the fluid flow rate through the pipes that can take action to control internal corrosion or retard it. A way to perform this type of analysis at the laboratory is using electrochemical cells through electrodes connected to a Potentiostat, which introduces an electrical signal in the system studied the same information obtained by analyzing the electrical response generated [3]. Rotating cylindrical electrode is used to generate fluid movement within cell causing this angular velocity.

Experiments require small amounts of fluid and electrochemical measurements can be made simultaneously. A rotating cylinder causes turbulence due to entrainment of the fluid on the surface [4]. T. Pérez et. al. [5] only focuses on the effect of plates and a concentric cylinder used as counter electrodes were simulated on a turbulent flow of a Rotating cylinder electrode. Therefore, this study aims in evaluating the corrosion rate of a steel pipe grade, caused by fluid flow containing an aggressive agent as H₂S in brine. For analysis of the distribution of the fluid on the steel (rotating cylindrical electrode) an ANSYS FLUENT simulation was performed and finally the corrosion products in the samples were studied using X-ray diffraction (XRD) and scanning electron microscopy (SEM) and Electron Dispersive X-ray (EDX) for mapping elements in the corrosion products, for observing the effect of the fluid on the corrosion rate of the steel.

2. EXPERIMENTAL PROCEDURE

The development of the present research is divided into two parts: mathematical simulation and electrochemical tests in the laboratory.

2.2 Mathematical Simulation

A mathematical simulation was performed first to design the electrochemical cell and the rotary cylinder in SolidWorks 2013, as shown in Figure 1. Further this geometry was used for the simulations in ANSYS FLUENT 14.5 and two phases were considered. Phase 1 is the kerosene and the brine; phase 2. Stirring at different times (10, 30 and 60 seconds) for each rate of agitation simulations were made, from 500 to 6000 rpm. It was observed that the two phase mixture within cell showed no significant changes in mass dispersion after 60 seconds.

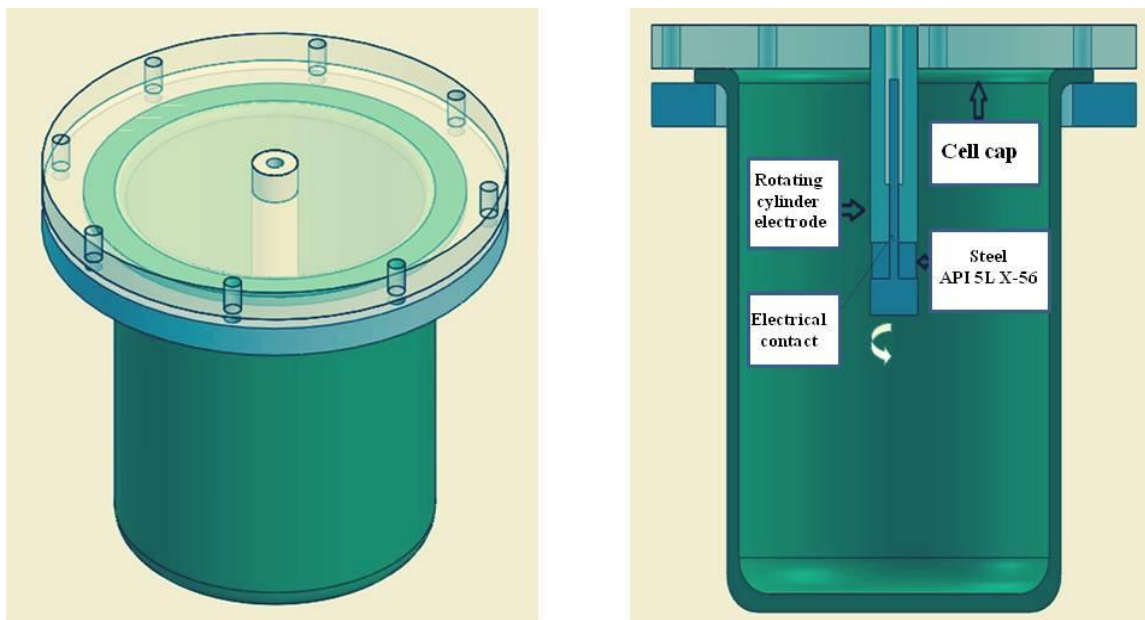


Figure 1. Design of the electrochemical cell employed in solid works.

2.3 Electrochemical Test

2.3.1 Test Environment.

The test solution was a brine prepared according to NACE standard 1D-196 with 106.5789 g/l NaCl, 4.4773 g/l $\text{CaCl}_2 \cdot 2\text{H}_2\text{O}$, 2.061 g/l $\text{MgCl}_2 \cdot 6\text{H}_2\text{O}$, 10% of kerosene and 1387.2 ppm of hydrogen sulfide (H_2S) were added. The temperature of the solution was 35°C and 45°C. The test solution was deaerated with nitrogen gas for a period of 30 minutes according to ASTM G59-97 to remove dissolved oxygen.

2.3.2. Experimental set up.

A cell made of Pyrex glass heated was used. Cylindrical tests specimens were cut off from API 5L-X56 (0.19% C, 0.63% Mn, 0.26% Si, 0.03% S, 0.024% P, Fe as the balance) steel pipe of 11 mm or more in thickness along the longitudinal direction. The total area exposed of the working electrode was 3.5 cm² for static and dynamic tests. The reference electrode was saturated calomel electrode, and two auxiliary electrodes of sintered graphite rods were used. Before each experiment the working electrode was polished with grade 600 silicon carbide paper, cleaned with deionized water and degreased with acetone. All electrochemical tests were performed on recently cleaned samples and fresh solutions.

2.3.3. Rotating cylindrical electrode (RCE).

The RCE was a computer controlled type, made by Radiometer Analytical, type EDI 10000 and connected to a Potentiostat/Galvanostat. The working electrode rotational speeds used in this study were varied from 0 to 6000 rpm, with increments of 500 rpm.

2.3.4. Corrosion rate measurements.

A “Standard Test Method for Conducting Potentiodynamic Polarization Resistance Measurements” (ASTM G59-97 (Reapproved 2003)) was applied by means of the commercial software POWER SUIT of Princeton Applied Research by using a Potentiostat/Galvanostat Princeton Applied Research model 263A (over the range of ± 20 mV). The polarization curves were obtained at a rate of 0.166 mV per second. The corrosion rate was obtained as a function of flow rate for the steels used in brine added with 10% of kerosene in presence of H₂S at 35°C and 45°C.

2.4. Characterization of corrosion products by SEM.

The surface morphology and composition of the corrosion products formed on electrode surface was characterized and analyzed using a scanning electron microscopy (SEM) Jeol JSM 6300 operated at 20 kV, 220 μ A and with a work distance of 39 mm.

2.5 Structural characterization by XRD

X-ray diffraction (XRD) was used to identify the corrosion products formed on API 5L-X56 steel, within a scanned range from 20° to 90° and a step width of 0.02°, using a D8 Focus Bruker diffractometer with Cu K α radiation.

3. RESULTS AND DISCUSSION

3.1 Mathematical simulation

As mentioned previously, simulations at different times and different agitation speeds, beginning at 500 rpm with increments of 500 rpm down to 6000 rpm were carried out. The most representative results of the mathematical simulation are shown in Figures 2 to 4. 2a) and 2b) depicting the volume fraction contours of the velocity vectors obtained at 500 rpm after 60 seconds of shaking. It is observed that the phases do not mix and the velocity vectors show very low speeds (0.254 m/s) while maintaining laminar flow in this stage Figures 3 a) and b) correspond to rotation speeds of 3000 rpm.

It is observed that the brine starts mixing with kerosene causing a variation in the corrosion rate, because kerosene mainly acts as a corrosion inhibitor. The velocity vectors reach 0.748 m/s.

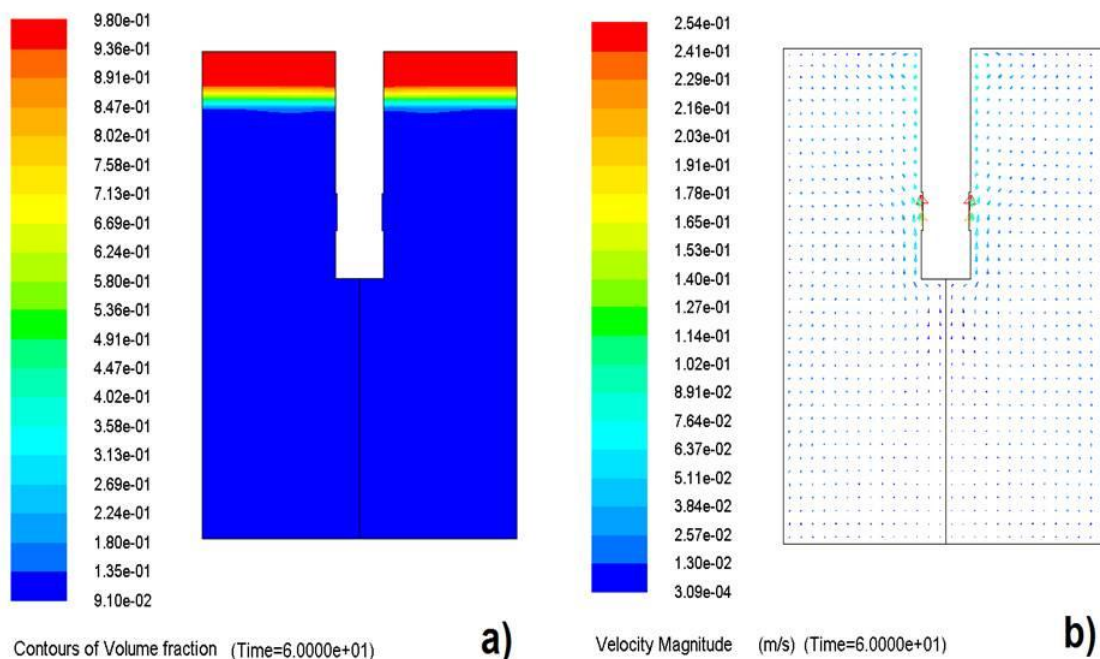


Figure 2. a) Contours of volume fraction and b) velocity vectors at 500 rpm.

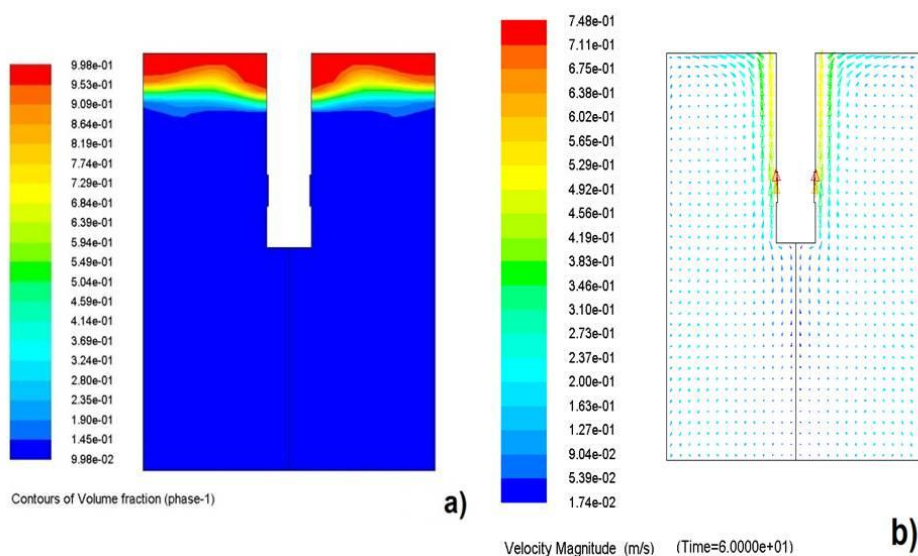


Figure 3. a) Contours of volume fraction and b) velocity vectors at 3000 rpm.

The volume fraction contours for a rotation speed of 6000 rpm are shown in Figure 4 a) observing that the kerosene and the brine are completely mixed and the mixture completely covers the stirrer of the RCE and therefore the steel sample.

The results showed the presence of turbulent Taylor Vortex flow in the bottom of the cell was reported by Rivero et al. [6]. The vectors show a speed of 1.37 m/s on the steel in Figure 4 b).

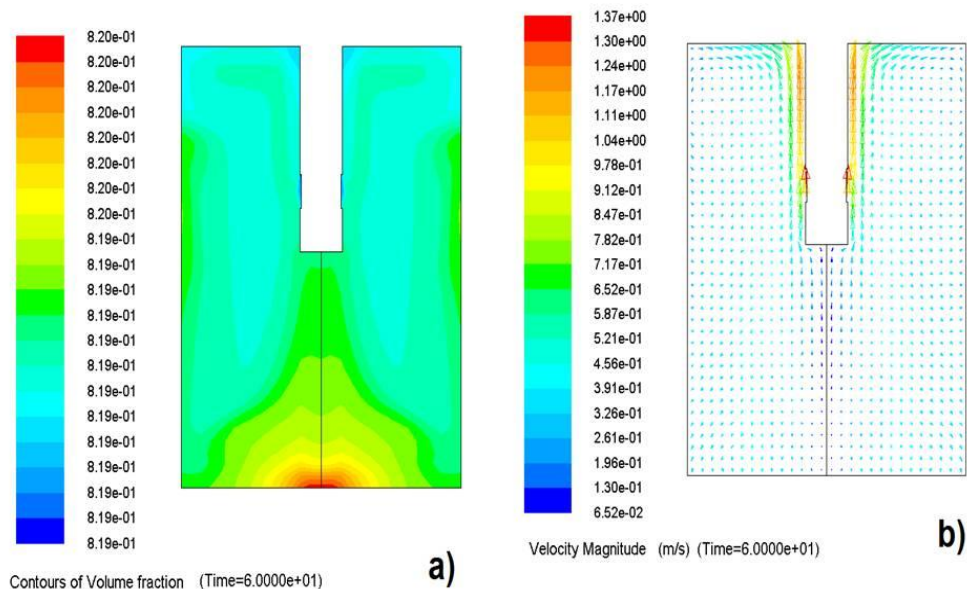


Figure 4. a) Contours of volume fraction and (b) velocity vectors at 6000 rpm.

3.2 Microstructure

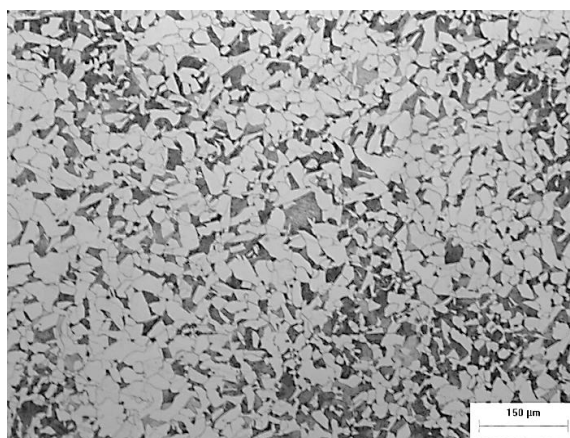


Figure 5. Micrograph of the microstructure for API 5L X-56 steel.

Figure 5 shows the microstructure of the steel, in this case it can be seen the presence of pearlite (dark phase) in a ferritic matrix (light phase). This is in agreement with similar microstructure obtained by others [7-9]. The microstructure is considered to have an important effect on how firmly the corrosion scale sticks to the surface. The adherence of the corrosion product film and hence its protectiveness, has often been related to the presence of iron carbide and its morphology (laminar, globular, etc). However, the accumulation of carbides in the corrosion product has been seen as the cause of increasing corrosion rate over time of exposure for ferritic perlitic (F/P) steels [10].

3.3 Linear polarization curves.

3.3.1 Comparison of corrosion rates as a function of flow rates for API 5L X-56 steel in presence of H₂S at 35 and 45°C

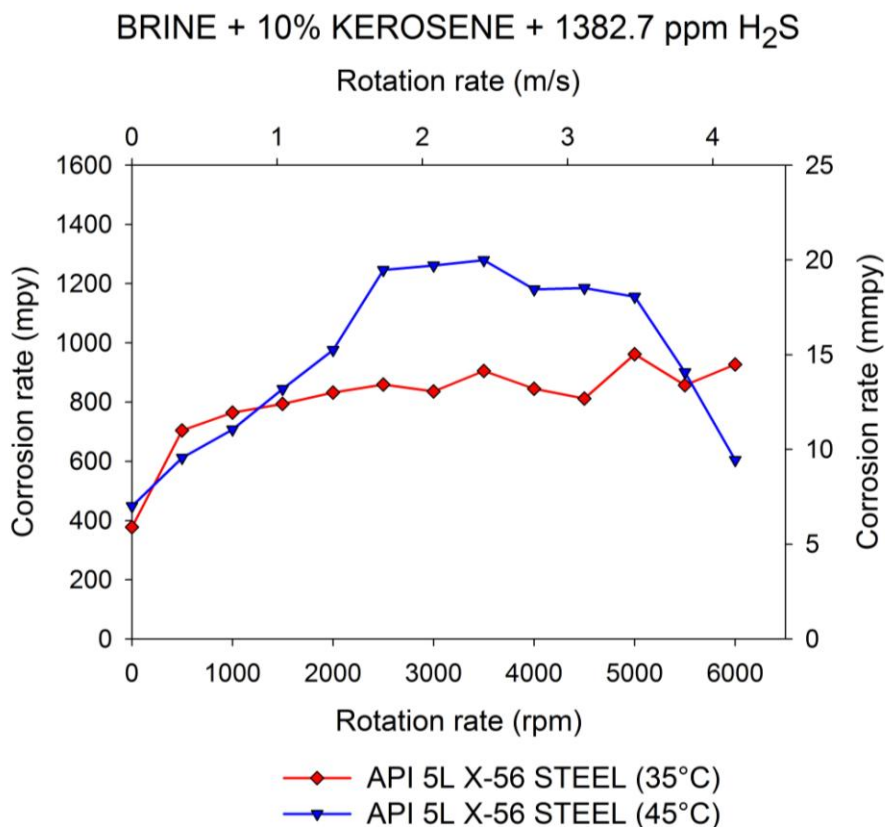


Figure 6. Corrosion rate comparison as a function of the flow rate for the API 5L X-56 steel in brine added with kerosene in presence of H₂S at 35 and 45°C.

In Figure 6 the results for the rate of corrosion of steel API 5L X-56 in a brine added with kerosene and H₂S at 35°C and 45 ° C, are compared to assess which has the best behavior with respect to corrosion. From these results it was observed that for both temperatures from the beginning corrosion rate is increased with increasing flow rate (this variation by the dependence of the corrosion rate on the flow velocity is generally attributed to a change by the corrosion mechanism [11]). Up to a rotation speed of 3500 rpm to 6000 rpm at 45°C corrosion rate always tends to decrease, thus suggesting that the corrosion products formed on the surface are more stable. At 35°C there is an increase in the corrosion rate which indicates that there was a detachment of corrosion products formed due to the same action of the flow (inducing movement to the fluid, the wall shear stresses decrease the thickness of this layer [12], which lead to an increase of the corrosion rate), so these may not be as stable or have a good adherence as the corrosion products at the other temperature (45°C).

It was observed that API 5L X-56 steel has a better performance in terms of corrosion rate, attributed to its more uniform formation of corrosion products (mixture of oxides and sulfides).

3.4 SEM surface characterization

Steel corrosive deposits form a solution that is mainly composed of insoluble products, undissolved constituents and trace amounts of alloying elements. They formed various oxides and sulfides as result of the corrosion process on the metal, under certain conditions or the type of medium used.

Figures 7 (a) and (b) are SEM micrographs of the corrosion products formed on surfaces of the API 5L X-56 steels at 35°C, (c) and (d) at 45°C. In both cases a layer of amorphous corrosion products on the surface begins to be visible, highlighting the API 5L X-56 steel at 45°C.

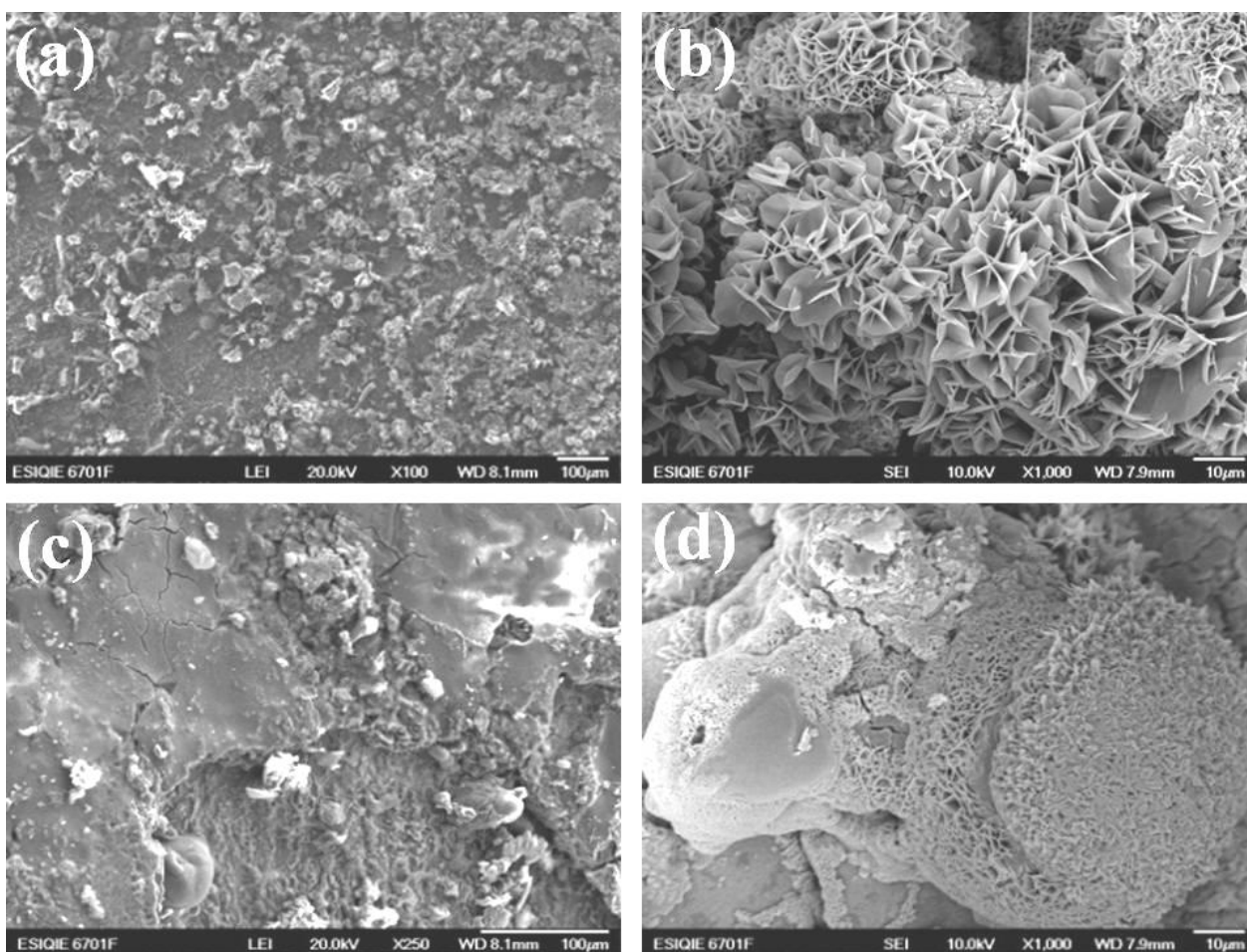


Figure 7. SEM images obtained after the formation of corrosion products on the API 5L X-56 steel surface (a),(b) 35°C and (c),(d) 45°C.

Figure 8 and 9 show mapping images of API 5L X-56 steel surface produced by EDX at 30 and 45°C in brine added with kerosene and H₂S; where the elements O, S and Fe are identified. These elements on the surface indicate the presence of a protective layer of FeO, Fe₂O₃, Fe₃O₄ or some sulfides as mackinawite (FeS_{1-x}), film formation (corrosion products) as reported in the literature [13-15]. In the case of 45°C, it can be shown that is very strong the presence of these corrosion products over surface of the steel.

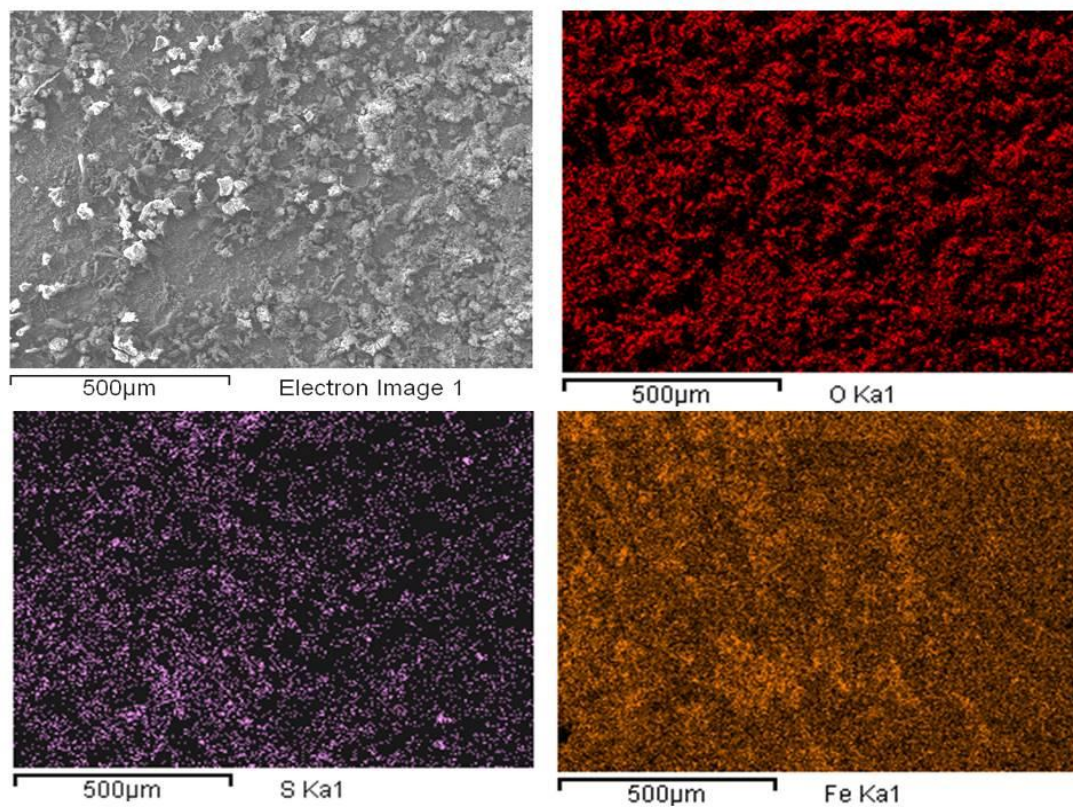


Figure 8. EDX mapping results of API 5L X-56 steel at 35°C.

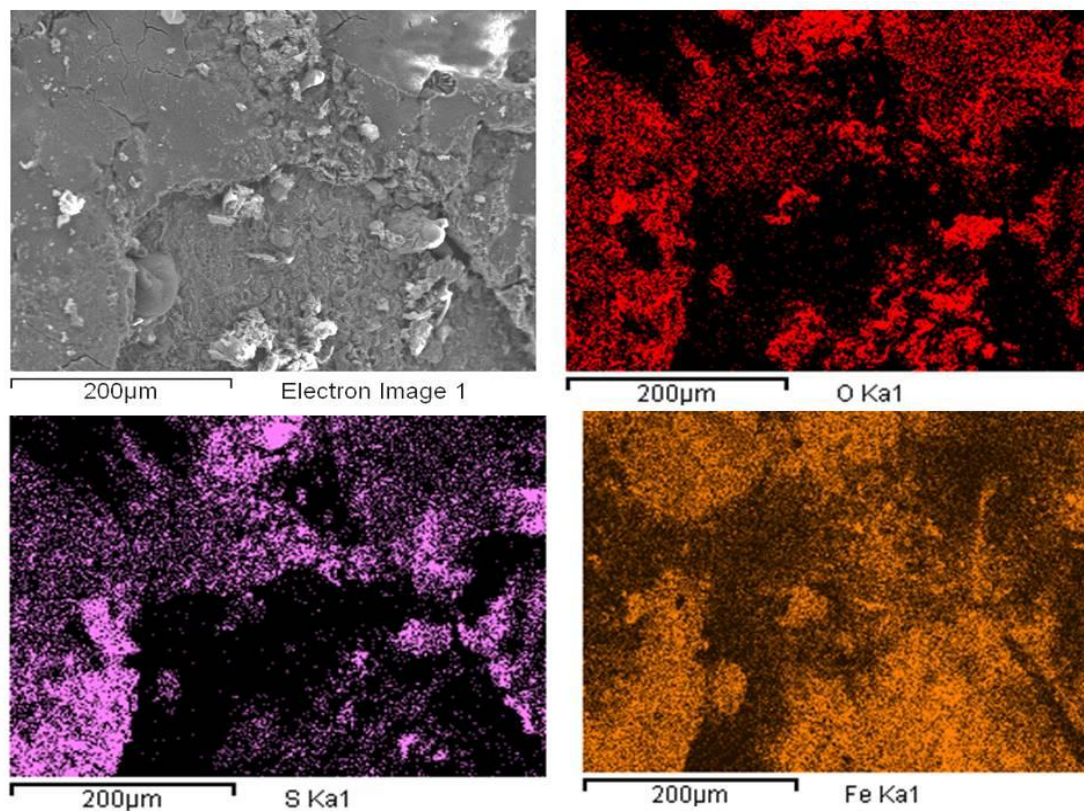


Figure 9. EDX mapping results of API 5L X-56 steel at 45°C.

3.5 XRD Characterization of corrosion products

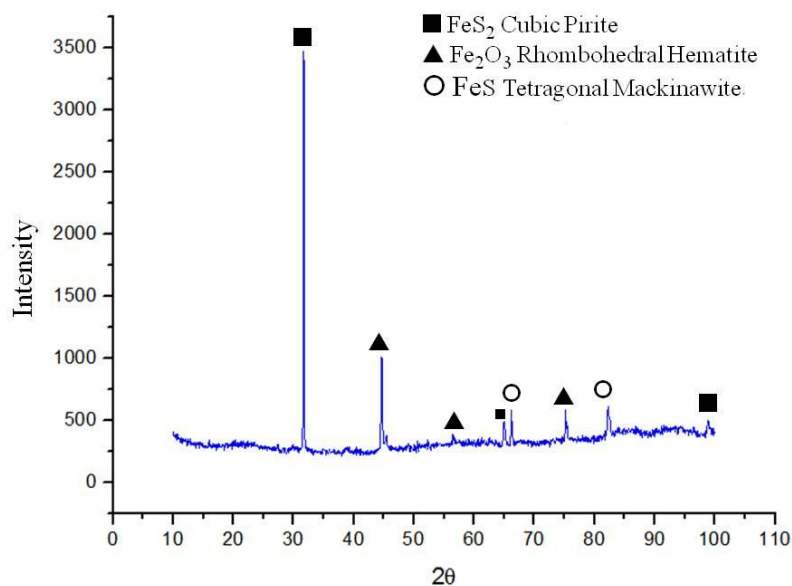


Figure 10. X-ray diffraction analysis (XRD) of corrosion products in API 5L X-56 steel surface in brine added with kerosene and H₂S at 45°C.

X-ray diffraction analysis have shown that the corrosion products formed Figure 10 for both temperatures were similar, according to A. Hernández et al [16] where API 5L-X56 is formed with a mixture of oxides and sulfurs. At both temperatures there are mainly formed oxides as Hematite (Rhombohedral), Mackinawite (Tetragonal) and Pirite (Cubic) as reported Y. Qi et al. [17] for A350LF2 steel in similar Hydrogen Sulfide enviroment. Mackinawite is a common mineral composed of tetragonal crystal and is considered a protective layer. The differences of the crystal structures of iron sulfide are due to the corrosive medium differences [18]. The presence of some oxides as Fe₂O₃ and Fe₃O₄, partially protects the steel surfaces from further dissolutions and leads in turn to the appearance of a passive region on the behavior of the corrosion rate as reported by E.S. Sherif et al [19]. For API 5L X-56 at 45°C, although it forms a greater quantity of corrosion products and suffer some detachment by the action of flow.

4. CONCLUSIONS

By mathematical model it was observed that fluid behavior to a low stirring speed shows a laminar flow, but as increasing the speed rotation of the cylindrical electrode, until reaches to 6000 rpm, it leads turbulent conditions together with the presence of a vortex in the bottom of the electrochemical cell employed. Kerosene also acts as corrosion inhibitor because of the oil phase, which interacts with the electrode surface.

Generally corrosion rate tends to increase with a higher rate of electrode rotation, but particularly tends to decrease at 45°C (3500-6000 rpm), due to a greater presence of corrosion products formed in steel surface. The corrosion products are composed of a mixture of oxides with sulfides. Therefore, in both temperatures employed in this research, the corrosion products acts as a protective film against the corrosion process, being in the API 5L-X56 yielding best behavior for having more sulfides than oxides.

ACKNOWLEDGEMENTS

The authors are also grateful for the financial support to the group of Pipeline Integrity Analysis (GAID-IPN), CONACYT and SIP-IPN.

References

1. D. R. Rubén, G. M. Ricardo, M. F. Juan, *Afinidad*, 62 (2005) 448.
2. S. Netic, S. Postlethwaite, *Corrosion*, 52 (1996) 280.
3. P. B. Dario, S. S. M. Teresa, *Revista Facultad de Ingeniería*, 37 (2006) 141.
4. M. A. Carlos, M. F. Leonardo, R. C. N. Shirley, P. Y. Dario, V. Q. Custodio, *Scietia Et Technica* (2007) 151.
5. T. Pérez, N. José L., *Int. J. Electrochem. Sci.*, 8 (2013) 4690.
6. E. P. Rivero, P. Granados, F. F. Rivera, M. Cruz and I. González, *Chem. Eng. Sci.*, 65 (2010) 3042.
7. R. Dong, I. Sun, Z. Liu, X. Wang and Q. Liu, *Journal of Iron and Steel Research International*, 15 (2008) 71
8. D. Clover, B. Kinsella, B. Pejicic and R. De Marco, *Journal of Applied Electrochemistry*, 35 (2005) 139.
9. C.W. Du, X.G. Li, P. Liang, Z.Y. Liu, G.F. Jia and Y.F. Cheng, *Journal of Materials Engineering and Performance*, 18 (2009) 216.
10. D. A. López, T. Pérez, S. N. Simison, *Materials and Design*, 24 (2003) 561.
11. J. Liu, Y. Lin, X. Yong, X. Li, *Corrosion*, 61 (2005) 1061.
12. Y.S. Choi, J.J. Shim, J.G. Kim, *Journal of Alloys and Compunds*, 391 (2005) 162.
13. R. N. Tuttle, R. D. Kane, *A Compilation of Classic Papers*, NACE, Houston, Texas (1981).
14. F. H. Meyer, O. L. Riggs, R. L. McGlasson, J. D. Sudbury, *Corrosion*, 14 (1958) 69.
15. S. N. Smith, E. J. Wright, *Corrosion/94*, Paper no. 011 (Houston, TX: NACE International, 1994).
16. A. Hernández-Espejel, M.A. Dominguez-Crespo, R. Cabrera-Sierra, C. Rodriguez-Meneses, E.M Arce-Estrada, *Corros. Sci.*, 52 (2010) 2258.
17. Y. Qi, H. Luo, S. Zheng, Ch. Chen, Z. Lv, M. Xiong, *Int. J. Electrochem. Sci.*, 9 (2014) 2101.
18. L. J. Yan, L. Niu, H. C. Lin, W. T. Wu, S. Z. Liu, *Corros. Sci.*, 41 (1999) 2305.
19. El-Sayed M. Sherif, Abdulhakim A. Almajid, Khalil Abdelrazek Khalil, Harri Junaedi and F.H. Latief, *Int. J. Electrochem. Sci.*, 8 (2013) 9360.